Geophysical Research Letters

RESEARCH LETTER
10.1029/2021GL096202

Examining the Wind Shear Theory of Sporadic E With ICON/MIGHTI Winds and COSMIC-2 Radio 2 Occultation Data

Y. Yamazaki[1], C. Arras[1], S. Andoh[2], Y. Miyoshi[3], H. Shinagawa[4], B. J. Harding[5], C. R. Englert[6], T. J. Immel[5], S. Sobhkhiz-Miandehi[1,7], and C. Stolle[8]

[1]GFZ German Research Centre for Geosciences, Potsdam, Germany, [2]Graduate School of Science, Kyoto University, Kyoto, Japan, [3]Department of Earth and Planetary Sciences, Kyushu University, Fukuoka, Japan, [4]National Institute of Information and Communication Technology, Tokyo, Japan, [5]Space Sciences Laboratory, University of California, Berkeley, Berkeley, CA, USA, [6]Space Science Division, U.S. Naval Research Laboratory, Washington, DC, USA, [7]Faculty of Science, University of Potsdam, Potsdam, Germany, [8]Leibniz Institute of Atmospheric Physics at the University of Rostock, Kühlungsborn, Germany

Abstract The wind shear theory is widely accepted as an explanation for the formation of a sporadic E (Es) layer, but the direct comparison of Es with the local wind shear has been limited due to the lack of neutral wind measurements. This study examines the role of the vertical wind shear for Es, using signal-to-noise ratio profiles from COSMIC-2 radio occultation measurements and concurrent measurements of neutral wind profiles from the Ionospheric Connection Explorer. It is observed that the Es occurrence rate and average S4 index are correlated with the negative vertical shear of the eastward wind, providing observational support for the wind shear theory. Es can be observed even when the vertical wind shear is positive, which is interpreted as metallic ion layers generated at an earlier time.

Plain Language Summary Sporadic E (Es) is anomalous radio propagation resulting from intense clouds of ionization at heights of the E-region ionosphere (90–120 km). The formation of an Es layer is generally attributed to the vertical wind shear, which can move metallic ions in the vertical direction by the Lorentz force. According to the wind shear theory, a negative shear of the eastward wind is effective in converging the metallic ions into a thin layer to produce Es. Although previous observations and modeling studies have supported the theory to various degrees, the direct comparison of Es with the vertical wind shear has been limited due to sparse observations of neutral winds at E-region heights. Neutral wind profiles from the Ionospheric Connection Explorer mission, together with Es data from COSMIC-2 radio occultation measurements, provide an opportunity to fill this knowledge gap. Direct comparisons of these measurements reveal that the Es occurrence rate is higher and lower for larger negative and positive wind shears, respectively, providing observational evidence for the wind shear theory.

Key Points:

- Conjunction observations of sporadic E (Es) from COSMIC-2 and neutral wind profiles from Ionospheric Connection Explorer/Michelson Interferometer for Global High-Resolution Thermospheric Imaging are analyzed
- Es occurrence rate correlates with the negative vertical shear of eastward wind, providing observational evidence for the wind shear theory
- Es can be observed even when the vertical shear of the local eastward wind is positive

Correspondence to:
Y. Yamazaki,
yamazaki@gfz-potsdam.de

Citation:
Yamazaki, Y., Arras, C., Andoh, S., Miyoshi, Y., Shinagawa, H., Harding, B. J., et al. (2022). Examining the wind shear theory of sporadic E with ICON/MIGHTI winds and COSMIC-2 Radio 2 occultation data. *Geophysical Research Letters*, *49*, e2021GL096202. https://doi.org/10.1029/2021GL096202

Received 16 SEP 2021
Accepted 17 DEC 2021

1. Introduction

Metallic ion layers are commonly observed in the ionosphere. In particular, those which occur at E-region heights show high plasma concentrations, and they can cause anomalous high frequency (HF) radio propagation, known as Es. The characterization of the phenomenon and the formation mechanism for Es layers have been a subject of study for many decades (see, e.g., reviews by Haldoupis, 2011; Mathews, 1998; Whitehead, 1989). Observations of Es have been made using various instruments and techniques, including ionosondes (e.g., Taguchi, 1961), sounding rockets (e.g., Smith, 1966), incoherent scatter radars (e.g., Miller & Smith, 1978), lidars (e.g., Gardner et al., 1993), and radio occultation measurements (e.g., Hocke et al., 2001). It is now well established that Es layers occur most frequently at mid latitudes (20°–50° latitude) in the summer hemisphere at altitudes of 90–120 km.

The formation of an Es layer requires the convergence of ion flux. The wind shear theory (Axford, 1963; Whitehead, 1961) suggests that the required ion flux convergence can be realized by the vertical shear of horizontal neutral winds. The following simple expression can be obtained for the vertical component of the ion velocity, under the assumption of balance between the Lorentz force due to ion motions across the ambient geomagnetic field and the frictional force due to ion-neutral collisions (e.g., Haldoupis, 2011):

$$w_i = \frac{1}{1+r^2}\left(rU_m \cos I - V_m \cos I \sin I\right) \quad (1)$$

with

$$r = \frac{\nu_i}{\Omega_i}, \tag{2}$$

where w_i is the vertical ion velocity, ν_i is the ion-neutral collision frequency, Ω_i is the ion gyrofrequency, I is the magnetic inclination, and U_m and V_m are neutral wind velocities in magnetic eastward and northward directions, respectively. In (1), the relative contribution of U_m and V_m to w_i depends on r, which decreases with height. In the height range of 90–120 km, where Es is most commonly observed, w_i is dominated by the contribution of U_m. Thus, the vertical convergence of the ion flux $-\frac{\partial}{\partial z}(N_i w_i)$, where N_i is the ion number density, is controlled by the vertical gradient of the zonal wind. The implication is that an Es layer should preferably occur where the negative gradient of the eastward wind is large.

Es layers are composed primarily of metallic ions such as Fe^+ and Mg^+, which have a relatively long lifetime and are abundant in the lower thermosphere due to meteor ablation (Kopp, 1997). Major ion species of the E-region ionosphere such as NO^+ and O_2^+ make little contribution to Es layers, as they cannot maintain high concentration due to a short lifetime relative to the convergence time. Modeling studies have demonstrated that thin and intense metallic ion layers can form in the E region under the presence of proper vertical wind shear, supporting the wind shear theory (e.g., Andoh et al., 2020; Carter & Forbes, 1999; Huba et al., 2019; MacLeod et al., 1975; Resende et al., 2016).

Direct observational evidence for the wind shear theory is limited due to the lack of neutral wind measurements from the lower thermosphere. Es layers mostly occur above the height range where ground-based radars can reliably determine the wind velocity (e.g., Jacobi & Arras, 2019). Sounding rockets have sometimes provided simultaneous measurements of plasma densities and neutral winds suitable for testing the wind shear theory. Some studies found Es layers near the height of a strong negative shear of the eastward wind, supportive of the wind shear theory (e.g., Bishop et al., 2005; Larsen et al., 1998; Pfaff et al., 2020). However, Hall et al. (1971) observed an Es layer with a positive shear, contrary to the wind shear theory. Moreover, Liu et al. (2018) compared the vertical wind shear observed by the TIMED satellite and Es derived from radio occultation measurements, to find only a weak correspondence between the wind shear and Es observations. Thus, the relationship between the wind shear and Es is yet to be established by observations.

Recently, a large number of neutral wind measurements from the Ionospheric Connection Explorer (ICON) mission (Immel et al., 2018) and concurrent Es detection by the COSMIC-2 radio occultation (Yue et al., 2014) have become available, providing an opportunity for direct comparison of Es with the local wind shear. The main objective of this study is to clarify the relationship between the wind shear and Es using these data. We also use the whole atmosphere model, Ground-to-Topside Model of Atmosphere and Ionosphere for Aeronomy (GAIA) (Jin et al., 2011), to support the validation of ICON wind data. Brief descriptions of the COSMIC-2 and ICON data as well as the GAIA model are given in the following section.

2. Data and Model

Radio occultation is a powerful remote-sensing technique for atmospheric and ionospheric soundings (e.g., Hajj et al., 2002; Wickert et al., 2009). For this study, we use radio occultation data from the COSMIC-2 satellite constellation (Anthes & Schreiner, 2019), which consists of six satellites with a 24° inclination orbit at an initial altitude of 720 km. COSMIC-2 radio occultation receivers provide up to several thousand signal-to-noise ratio (SNR) profiles per day (Schreiner et al., 2020), covering the E region at latitudes between 45°S and 45°N and up to an altitude of ∼130 km with a vertical resolution of ∼25 m. SNR is sensitive to the vertical gradient of the plasma density. The plasma density gradient due to Es is considered to be the primary source of scintillation in SNR at E-region heights. In previous studies, SNR data from various satellite missions have been used to study Es layers (Arras et al., 2008; Hocke et al., 2001; Wu et al., 2005).

For each COSMIC-2 SNR profile, the Es occurrence is evaluated and the S4 scintillation index (or simply S4 index) is derived. The method used is essentially the same as that previously described by Arras and Wickert (2018) for studying Es with radio occultation data from the COSMIC satellite constellation (Anthes et al., 2008). Briefly, the detection of Es layers is based on profiles of the standard deviation of SNR calculated using a 2.5-km sliding window. A profile is considered to contain an Es layer if the maximum standard deviation exceeds the threshold

value of 0.2 and the large standard deviation (>0.2) is confined within a layer of maximum 15-km thickness. In this way, large plasma density gradients associated with Es (irrespective of the ion composition) can be detected. The S4 index is computed using 100 SNR data points around the height of the maximum SNR fluctuation. Studies found a correlation between the S4 index derived from COSMIC SNR data and the blanketing frequency of Es layer (*fb*Es) observed by ionosondes (Arras & Wickert, 2018; Resende et al., 2018). *fb*Es corresponds to the maximum electron density of the Es layer. It is noted that there are occasionally SNR profiles that are highly disturbed at all heights, which are likely due to a technical issue. Such "bad data," accounting for ∼2%, are excluded from the analysis.

Neutral wind data are obtained from the Michelson Interferometer for Global High-Resolution Thermospheric Imaging (MIGHTI) (Englert et al., 2017) onboard ICON. MIGHTI measures Doppler shifts of the naturally occurring atomic oxygen airglow emissions to estimate the horizontal wind velocity. We use version 4 of the cardinal wind profiles from the green-line emission at 557.7 nm wavelength (Harding et al., 2017, 2021). Wind profiles cover the latitude range between 12°S and 42°N and the height range of approximately 90–180 km, with a vertical resolution of ∼3 km. At each height, magnetic eastward (U_m) and northward (V_m) components are derived from geographic eastward (U) and northward (V) components using the magnetic declination obtained from the International Geomagnetic Reference Field (Alken et al., 2021). U_m and V_m are mainly used for comparisons with COSMIC-2 Es data, while U is used for comparisons with GAIA predictions. It is noted that the ICON/MIGHTI results obtained with U_m and V_m are generally similar to those derived with U and V. It is also noted that since the ICON/MIGHTI data are from mid and low latitudes, similar results are obtained with U_m and $U_m \cos(I)$. We use only the ICON/MIGHTI data with "wind quality factor" equal to one, which corresponds to the best quality data. This largely eliminates the measurements taken near the South Atlantic Anomaly, which are contaminated by radiation impacting the MIGHTI detectors.

A COSMIC-2 SNR profile and ICON/MIGHTI neutral wind profile are considered to be in "conjunction" if the spatial separation of the two is less than 2.5° in both latitude and longitude, and the temporal separation is less than 10 min in terms of the central time of the observations. Sometimes, more than one SNR profile is found for the same wind profile. In our statistical analysis, conjunctions are treated to be independent as long as the SNR profiles are different. The data during the period from June 2020 to May 2021 are used, and 10,751 conjunctions are detected.

Neutral wind velocities are also obtained from GAIA, which is a physics-based model of the coupled atmosphere-ionosphere system from the surface to the upper thermosphere/ionosphere (Jin et al., 2011). The model consists of the following three parts: a whole atmosphere general circulation model (GCM) (Miyoshi & Fujiwara, 2003), an ionosphere model (Shinagawa, 2011), and an electrodynamics model (Jin et al., 2008), which are coupled to one another. The model was run for the same period as our data set, that is, from June 2020 to May 2021. The whole atmosphere GCM below the height of 40 km was constrained with meteorological reanalysis, namely, the Japanese 55-year Reanalysis (JRA55) (Kobayashi et al., 2015) using a nudging technique (e.g., Jin et al., 2012). This way, the model is able to incorporate atmospheric tides that are generated in the lower atmosphere and propagate into the upper atmosphere (e.g., Miyoshi et al., 2017). Studies have shown that these tides play an important role for the daily variation of Es (e.g., Haldoupis et al., 2006).

3. Results and Discussion

Figure 1 presents examples of conjunction observations of COSMIC-2 SNR and ICON/MIGHTI wind profiles (magnetic eastward component). Vertically confined large fluctuations in SNR profiles indicate the presence of an Es. In the upper three panels, Es layers are seen at an altitude where the magnetic eastward component of the zonal wind decreases with height (i.e., the vertical wind shear is negative). Es layers in these results conform well to expectations from the wind shear theory.

In the lower left panel of Figure 1, an Es layer is seen at a height (∼113 km) of a negative wind shear, again supporting the wind shear theory. The SNR profile also indicates the presence of another Es layer at a lower height (∼93 km), for which there is unfortunately no wind measurement. Multiple-layer Es structures have been reported in the literature (e.g., Ejiri et al., 2019; Hall et al., 1971; Raizada et al., 2020). In the lower middle panel, a negative wind shear is seen at heights of 95–105 km, but with no apparent Es layer. The absence of an Es layer might be due to the lack of metallic ions. It is also possible that an Es layer is present but SNR fluctuations are not large

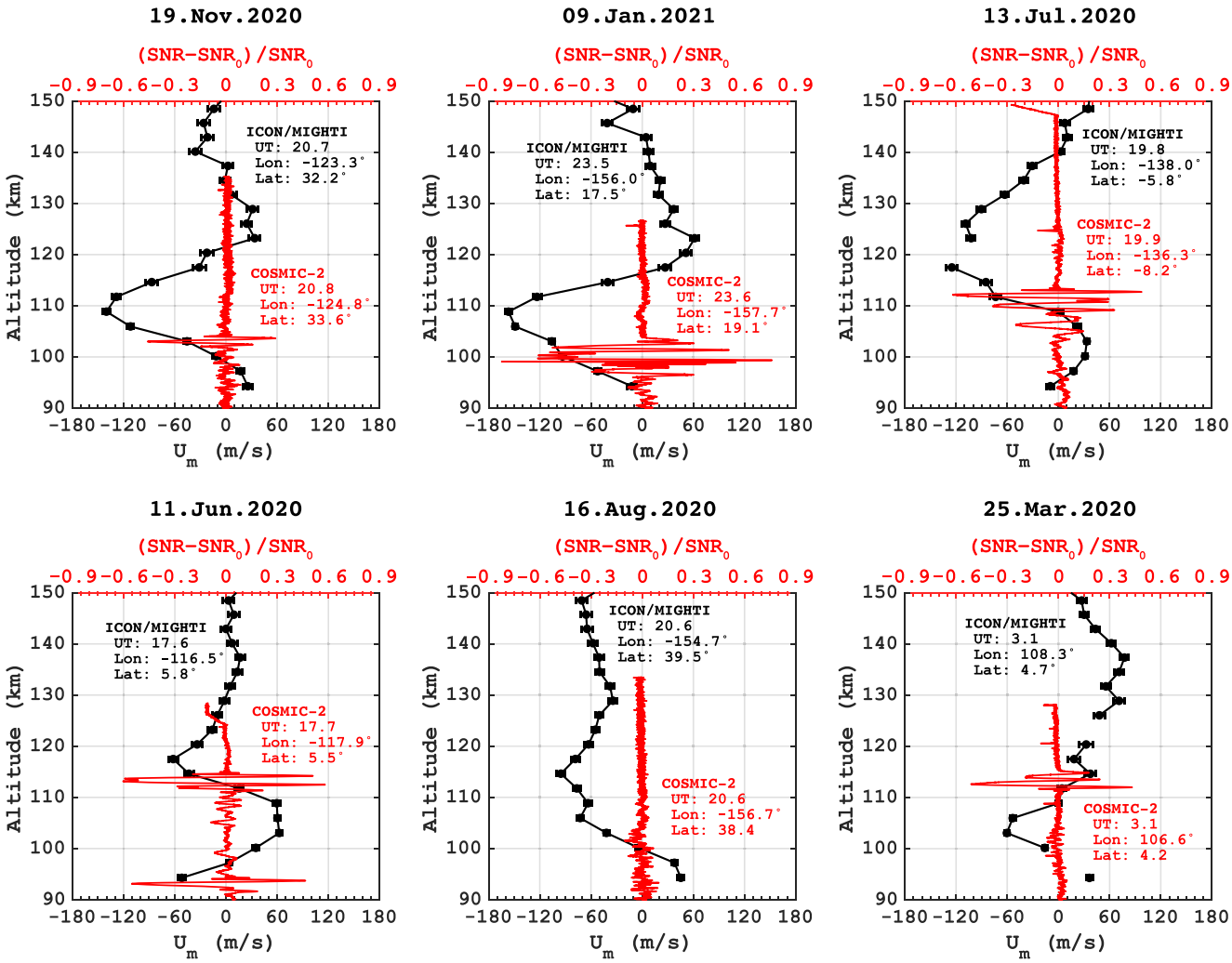

Figure 1. Examples of conjunction observations of COSMIC-2 signal-to-noise ratio (SNR) (red) and Ionospheric Connection Explorer/Michelson Interferometer for Global High-Resolution Thermospheric Imaging (ICON/MIGHTI) magnetic eastward wind (black) profiles. SNR_0 indicates the mean of SNR.

enough to be detected as Es. In the bottom right, an Es layer is seen at ∼112 km, but the vertical wind shear is not negative. A possible explanation is a surviving metallic ion layer generated at an earlier time. As mentioned, metallic ions have a long lifetime, and thus an Es layer would not immediately disappear when the polarity of the shear changes from a negative to a positive one.

Next, we compare daily-mean global climatologies of Es and vertical wind shear. For deriving the climatologies, not only conjunction observations, but also all other available COSMIC-2 and ICON data including all local times are used. Figure 2a shows the occurrence rate of Es over the height range 90–120 km for different periods. The following features can be noted: (1) the Es occurrence rate is higher in the summer hemisphere than in the winter hemisphere, (b) the Es occurrence rate is reduced over the magnetic equator, (c) the Es occurrence rate is also reduced in the southern mid latitudes between ±30° longitudes. These results are in good agreement with previous global observations (e.g., Arras et al., 2008). The enhanced Es occurrence rate in the summer hemisphere is due to the seasonal dependence of metallic ion densities and vertical wind shear (Chu et al., 2014; Haldoupis et al., 2007; Shinagawa et al., 2017). The reduced Es occurrence rate over the magnetic equator is thought to be due to the vertical electric field, which prevents the formation of an Es layer (e.g., Haldoupis, 2011). The reduced Es occurrence over the South Atlantic is understood in terms of relatively large magnetic inclination angle, which leads to a reduced vertical ion convergence over this region; see Equation 1.

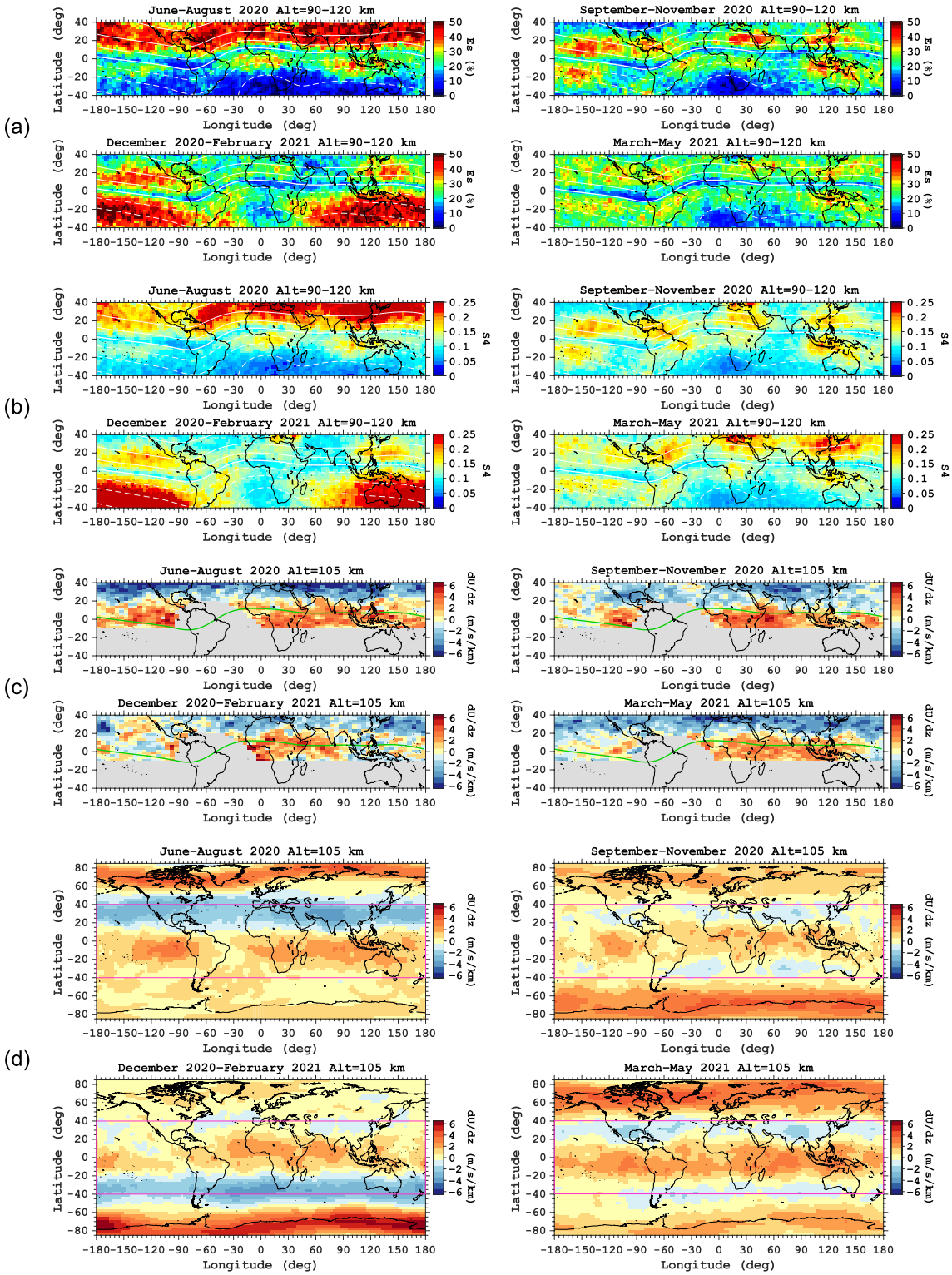

Figure 2. (a) The occurrence rate of sporadic E (Es) as derived from COSMIC-2 radio occultation data at 90–120 km during June–August 2020 (upper left), September–November 2020 (upper right), December 2020–February 2021 (lower left), and March–May 2021 (lower right). The white lines show contours of the magnetic inclination in 20° steps. (b) The same as (a) except for the S4 scintillation index. (c) The vertical shear of the Ionospheric Connection Explorer/ Michelson Interferometer for Global High-Resolution Thermospheric Imaging geographic eastward wind at 105 km. (d) The same as (c) but from the GAIA model.

Figure 2b displays the global distribution of the average S4 index in a similar format. The results are consistent with those in previous studies (Arras & Wickert, 2018; Chu et al., 2014; Yu et al., 2019). The distribution of the average S4 index and its seasonal variation are similar to those of the Es occurrence rate, as pointed out by Arras and Wickert (2018).

Figure 2c shows the vertical shear of the zonal wind (positive geographic eastward) at 105 km, the height around which the vertical wind shear is largest (e.g., Larsen, 2002). Mean values of the vertical wind shear are calculated using a sliding window of 5° × 10° in latitude and longitude. It is seen that there is no ICON/MIGHTI observation in the Southern Hemisphere poleward of ∼15°S. There is also no data around the South Atlantic Anomaly, as mentioned earlier. The vertical wind shear shows a consistent pattern of negative and positive wind shears poleward and equatorward of ∼20°N, respectively, in different seasons. The negative wind shear is strongest during June–August 2020, that is, local summer. This could make a contribution to the enhanced Es occurrence rate and average S4 index in local summer.

The vertical wind shear at 105 km obtained from GAIA is presented in panel (d). Mean values of the vertical wind shear are calculated from daily means at each grid point. Roughly speaking, the wind shear is positive over latitude ranges of 90°S–50°S, 20°S–20°N, and 50°N–90°N, and negative elsewhere. There is agreement between the ICON/MIGHTI results and GAIA predictions.

As a brief summary, the global patterns of the Es occurrence rate and average S4 index at 90–120 km are similar to each other, but they are only in partial agreement with the pattern of the vertical wind shear at 105 km. Since the results presented in Figure 2 contain the data from all local times, they are representative of the daily mean. Next, we address the local-time dependence of the Es occurrence rate, average S4 index, and vertical wind shear.

Figure 3a shows the local-time and altitude structures of the Es occurrence rate (upper left), average S4 index (upper right), vertical wind shear from ICON/MIGHTI (lower left), and vertical wind shear from GAIA (lower right) at 20°N–40°N during June–August 2020. The Es occurrence rate undergoes a semidiurnal variation above 105 km or so, while at lower altitudes, a diurnal variation is dominant. These diurnal and semidiurnal variations of Es are known to be associated with the vertical wind shear by atmospheric tides (Arras et al., 2009; Christakis et al., 2009). Downward phase propagation, which is a fundamental feature of upward propagating tides (e.g., Forbes, 1995), can be seen in the diurnal and semidiurnal Es variations. Tidal influences are also seen in the average S4 index, but the semidiurnal variation is not as evident as in the Es occurrence rate. Comparison of the Es occurrence rate with vertical wind shears from ICON/MIGHTI and GAIA suggests that the Es occurrence rate tends to be high at local times and altitudes where the vertical shear of the zonal wind is negative, which is consistent with the wind shear theory. There is reasonable agreement between ICON/MIGHTI observations and GAIA predictions, although the magnitude of the wind shear tends to be greater in the GAIA results.

Figure 3b show the same variables as panels (a) but at 10°S–10°N during September–November 2020. Compared with panel (a), both the Es occurrence rate and average S4 index are generally lower. Also, the agreement between the patterns of the Es occurrence rate and negative wind shear is not as good. For example, the Es occurrence rate is relatively high around 100–105 km at 14–18 LT, where the average vertical wind shear is positive. The results suggest that the daily variation of Es is not only due to tidal modulation of wind shear but also due to other mechanisms such as the daily variation of metallic ion density.

More direct comparisons between Es and vertical wind shear are made using only conjunction profiles of COSMIC-2 SNR and ICON/MIGHTI winds at altitudes of 90–120 km. In the upper panels of Figure 4, the Es occurrence rate (left) and average S4 index (right) are computed for every 2.5 m/s/km in the vertical shear of the magnetic eastward wind. The black lines show the results containing all periods, latitudes, and heights of observation, with linear fits indicated by magenta lines. Both the Es occurrence rate and average S4 index correlate almost linearly with the vertical wind shear. To assess the robustness of the results, we divided the data into two parts each having approximately half of the samples, and repeated the analysis for each group of data. The results obtained for different periods (blue solid and dashed lines) and for different ranges of latitude (green solid and dashed lines) are found to be similar to the results obtained with all the available data. Meanwhile, the results obtained for different height ranges (orange solid and dashed lines) are appreciably different. That is, the dependence of the Es occurrence rate and average S4 index on the vertical wind shear is more pronounced at higher (100–120 km) than lower (90–100 km) altitudes. The difference in the slope of a linear fit (not shown here) to the higher- and lower-altitude data is significant at the 95% confidence level. Such a significant difference is not found in the

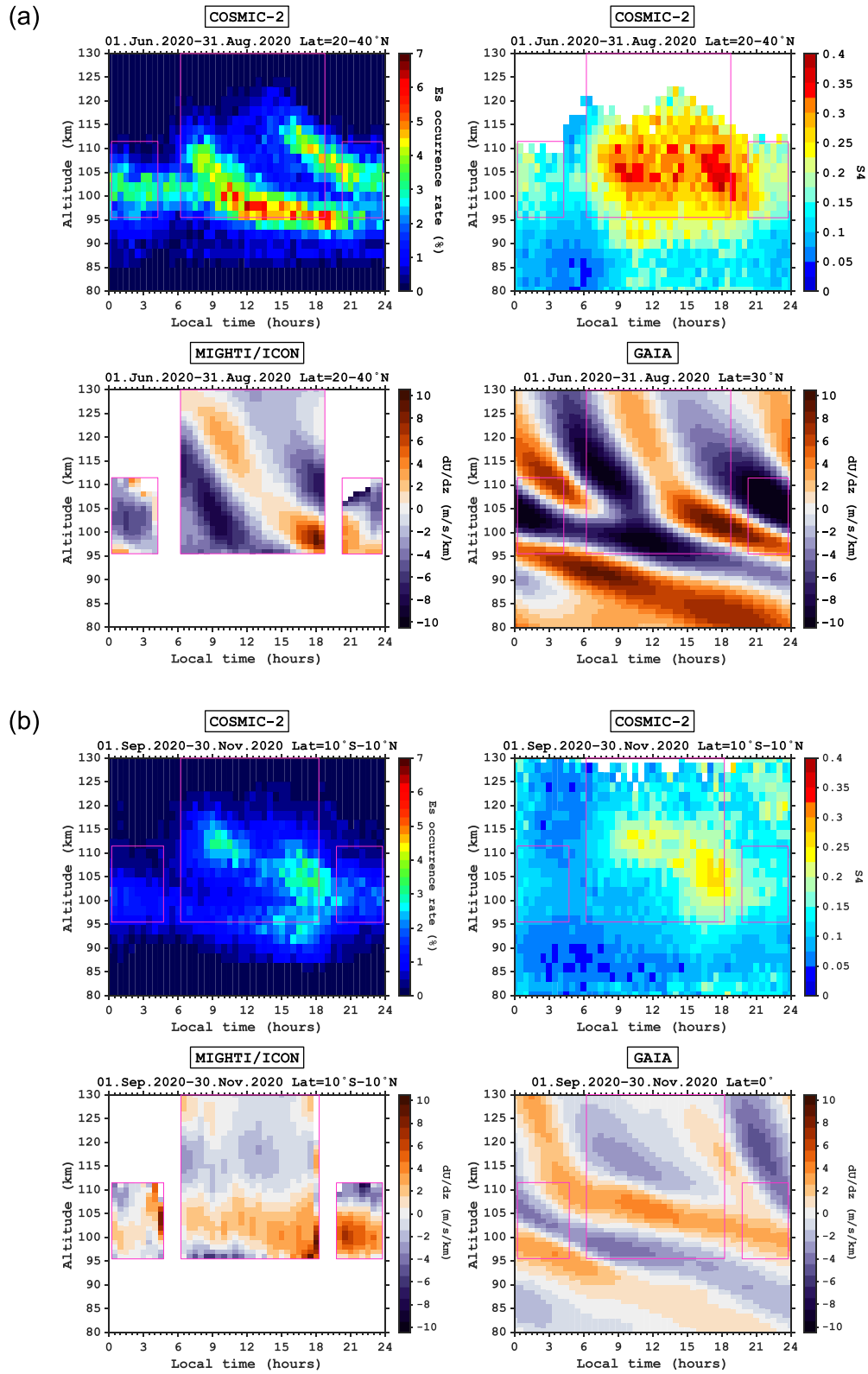

Figure 3. (a) The local time versus altitude plot of the COSMIC-2 sporadic E (Es) occurrence rate (upper left), S4 scintillation index (upper right), and vertical shears of the geographic eastward wind from Ionospheric Connection Explorer/ Michelson Interferometer for Global High-Resolution Thermospheric Imaging (ICON/MIGHTI) (lower left) and GAIA (lower right), at 20–40°N during June–August 2020. (b) The same as (a) except for 10°S–10°N during September–November 2020.

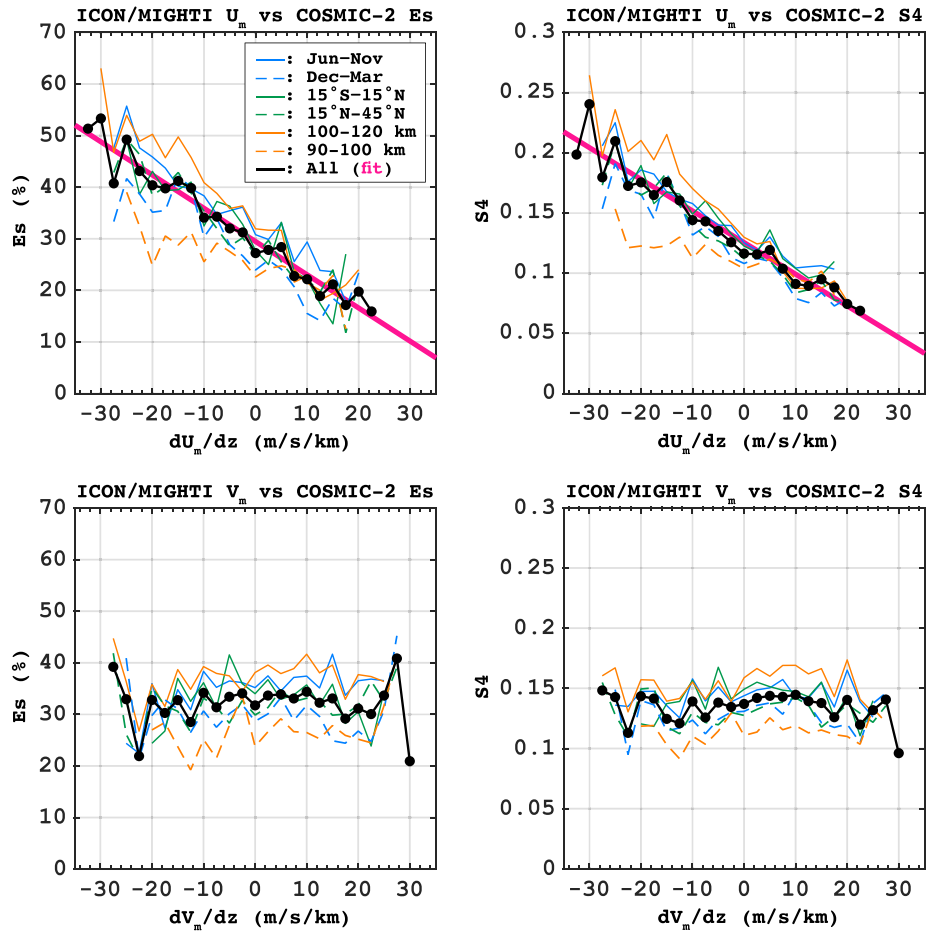

Figure 4. Dependence of the COSMIC-2 sporadic E (Es) occurrence rate (left) and S4 scintillation index (right) on the vertical shear of the Ionospheric Connection Explorer/Michelson Interferometer for Global High-Resolution Thermospheric Imaging (ICON/MIGHTI) magnetic eastward wind (top) and magnetic northward wind (bottom). The vertical shear of the meridional wind is multiplied by $I/|I|$, where I is the magnetic inclination. Black lines show the results containing all conjunction measurements at 15°S–45°N at 90–120 km heights during June 2020–May 2021. In the upper panels, linear fits are indicated by magenta lines. Other lines show the results obtained from a subset of the data. Blue solid and dashed lines correspond to the data from the first and last half of the period, respectively. Green solid and dashed lines correspond to the data at 15°S–15°N and 15°N–45°N, respectively. Orange solid and dashed lines correspond to the data at heights of 90–100 km and 100–120 km, respectively.

results obtained for different periods or latitudes. The reduced wind-shear influence at the lower altitudes can be explained as the consequence of frequent ion-neutral collisions in the lower E region, which suppress the Es formation by the wind shear mechanism, as numerically demonstrated by Andoh et al. (2021).

It may be noted that the Es occurrence rate at zero shear of the zonal wind is approximately 30%. Es without vertical wind shear can be due to a metallic ion layer generated at an earlier time. Such a surviving layer would be destroyed by the divergence of vertical ion motions induced by a positive wind shear. The destruction of the layer would be more rapid for a larger positive wind shear. This explains why the Es occurrence rate and average S4 index correlate not only with the negative shear but also with the positive shear of the zonal wind.

The lower panels of Figure 4 show that the vertical shear of the magnetic northward wind has little impact on the Es occurrence rate and average S4 index at 90–120 km. This is expected from the wind shear theory, which predicts that the vertical shear of the meridional wind plays a role only above 125 km or so (e.g., Haldoupis, 2011). It is noted that the vertical shear of the meridional wind in Figure 4 is multiplied by $I/|I|$, considering that the contribution of the meridional wind to Es is opposite in the magnetic Northern ($I > 0$) and Southern ($I < 0$) Hemispheres; see Equation 1. Our data set is not suitable for studying the statistical relationship between Es and

vertical wind shear above 120 km, as the detection of Es at such high altitudes is rather infrequent. The validity of the wind shear theory above 120 km requires further investigation.

4. Conclusions

This study has examined the wind shear theory of Es, for which existing evidence is mostly based on numerical simulations and sparse observations by sounding rockets. We have investigated the relationship between Es and vertical wind shear, using vertical profiles of COSMIC-2 radio occultation signal-to-noise ratio (SNR) and ICON/MIGHTI neutral winds. Global seasonal climatologies of the Es occurrence rate and S4 scintillation index derived from COSMIC-2 SNR profiles are in good agreement with those previously reported using other data, which validates the COSMIC-2 Es data. Also, the vertical shear of the ICON/MIGHTI zonal wind at E-region heights is in reasonable agreement with GAIA model predictions. Direct comparisons are presented for COSMIC-2 SNR and ICON/MIGHTI wind profiles for the latitude range of approximately 15°S–45°N and the altitude range of ∼90–120 km. The main results of the study may be summarized as follows:

1. Both the Es occurrence rate and average S4 index are correlated with the negative vertical shear of the eastward wind, providing observational support for the wind shear theory. The vertical shear of the meridional wind has little impact on Es for the height range of 90–120 km
2. The wind-shear effect on the Es occurrence rate and average S4 index is more pronounced above 100 km than below, consistent with the numerical work by Andoh et al. (2021). Below 100 km, frequent ion-neutral collisions suppress the formation of an Es layer by the wind shear mechanism
3. Es can be observed even in the absence of vertical wind shear. This can be due to the presence of surviving Es layers that are generated at an earlier time. The Es occurrence rate decreases with increasing magnitude of positive shear in the zonal wind, because a surviving metallic ion layer is destroyed by vertical ion flux divergence induced by the positive wind shear

Data Availability Statement

The COSMIC-2 radio occultation data (caL1Snr of level 1b, atmospheric excess phase profiles) are available from CDAAC: COSMIC Data Analysis and Archive Center: https://www.cosmic.ucar.edu/what-we-do/cosmic-2/data/. The ICON/MIGHTI Level 2.2 product Cardinal Vector Winds (Version 4) is accessible from the ICON website https://icon.ssl.berkeley.edu/Data.

Acknowledgments
We thank J. Rodríguez-Zuluaga for providing the IGRF data. We also thank the University Corporation for Atmospheric Research (UCAR) for providing the COSMIC-2 radio occultation data and the National Aeronautics and Space Administration (NASA) for providing the ICON/MIGHTI data. ICON is supported by NASA's Explorers Program through contracts NNG12FA45C and NNG12FA42I. GAIA simulation was mainly performed using the computer systems at Research Institute for Information Technology of Kyushu University. The JRA-55 meteorological reanalysis data sets are provided by the Japan Meteorological Agency (JMA). This work was supported in part by JSPS and DFG (grant YA-574-3-1) under the Joint Research Projects-LEAD with DFG (JRPs-LEAD with DFG). C. Arras acknowledges support by the DFG Priority Program Dynamic Earth, SPP 1788 under grant AR953/1-2.

References

Alken, P., Thébault, E., Beggan, C. D., Amit, H., Aubert, J., Baerenzung, J., & Zhou, B. (2021). International geomagnetic reference field: The thirteenth generation. *Earth Planets and Space*, *73*(1), 1–25. https://doi.org/10.1186/s40623-020-01281-4

Andoh, S., Saito, A., & Shinagawa, H. (2021). Temporal evolution of three-dimensional structures of metal ion layer around Japan simulated by a mid-latitude ionospheric model. *Journal of Geophysical Research: Space Physics*, *126*, e2021JA029267. https://doi.org/10.1029/2021JA029267

Andoh, S., Saito, A., Shinagawa, H., & Ejiri, M. K. (2020). First simulations of day-to-day variability of mid-latitude sporadic E layer structures. *Earth Planets and Space*, *72*(1), 1–9. https://doi.org/10.1186/s40623-020-01299-8

Anthes, R., Bernhardt, P., Chen, Y., Cucurull, L., Dymond, K., Ector, D., et al. (2008). The COSMIC/FORMOSAT-3 mission: Early results. *Bulletin of the American Meteorological Society*, *89*(3), 313–334. https://doi.org/10.1175/bams-89-3-313

Anthes, R., & Schreiner, W. (2019). Six new satellites watch the atmosphere over earth's equator, *EOS*, *100*. https://doi.org/10.1029/2019eo131779

Arras, C., Jacobi, C., & Wickert, J. (2009). Semidiurnal tidal signature in sporadic E occurrence rates derived from GPS radio occultation measurements at higher midlatitudes. *Annals of Geophysics*, *27*, 2555–2563. https://doi.org/10.5194/angeo-27-2555-2009

Arras, C., & Wickert, J. (2018). Estimation of ionospheric sporadic E intensities from GPS radio occultation measurements. *Journal of Atmospheric and Solar-Terrestrial Physics*, *171*, 60–63. https://doi.org/10.1016/j.jastp.2017.08.006

Arras, C., Wickert, J., Beyerle, G., Heise, S., Schmidt, T., & Jacobi, C. (2008). A global climatology of ionospheric irregularities derived from GPS radio occultation. *Geophysical Research Letters*, *35*(14). https://doi.org/10.1029/2008gl034158

Axford, W. (1963). The formation and vertical movement of dense ionized layers in the ionosphere due to neutral wind shears. *Journal of Geophysical Research*, *68*(3), 769–779. https://doi.org/10.1029/jz068i003p00769

Bishop, R., Earle, G., Larsen, M., Swenson, C., Carlson, C., Roddy, P., & Bullett, T. (2005). Sequential observations of the local neutral wind field structure associated with E region plasma layers. *Journal of Geophysical Research*, *110*(A4). https://doi.org/10.1029/2004ja010686

Carter, L., & Forbes, J. (1999). Global transport and localized layering of metallic ions in the upper atmosphere. *Annals of Geophysics*, *17*, 190–209. https://doi.org/10.1007/s00585-999-0190-6

Christakis, N., Haldoupis, C., Zhou, Q., & Meek, C. (2009). Seasonal variability and descent of mid-latitude sporadic E layers at Arecibo. *Annals of Geophysics*, *27*, 923–931. https://doi.org/10.5194/angeo-27-923-2009

Chu, Y.-H., Wang, C., Wu, K., Chen, K., Tzeng, K., Su, C.-L., et al. (2014). Morphology of sporadic E layer retrieved from COSMIC GPS radio occultation measurements: Wind shear theory examination. *Journal of Geophysical Research: Space Physics*, *119*(3), 2117–2136. https://doi.org/10.1002/2013ja019437

Ejiri, M. K., Nakamura, T., Tsuda, T. T., Nishiyama, T., Abo, M., Takahashi, T., & Wada, S. (2019). Vertical fine structure and time evolution of plasma irregularities in the Es layer observed by a high-resolution Ca+ lidar. *Earth Planets and Space*, *71*(1), 1–10. https://doi.org/10.1186/s40623-019-0984-z

Englert, C. R., Harlander, J. M., Brown, C. M., Marr, K. D., Miller, I. J., & Stump, J. E. (2017). Michelson interferometer for global high-resolution thermospheric imaging (MIGHTI): Instrument design and calibration. *Space Science Reviews*, *212*(1), 553–584. https://doi.org/10.1007/s11214-017-0358-4

Forbes, J. M. (1995). Tidal and planetary waves. The upper mesosphere and lower thermosphere: A review of experiment and theory. *Geophysical Monograph Series*, *87*, 67–87.

Gardner, C. S., Kane, T. J., Senft, D. C., Qian, J., & Papen, G. C. (1993). Simultaneous observations of sporadic E, Na, Fe, and Ca+ layers at Urbana, Illinois: Three case studies. *Journal of Geophysical Research*, *98*(D9), 16865–16873. https://doi.org/10.1029/93jd01477

Hajj, G. A., Kursinski, E., Romans, L., Bertiger, W., & Leroy, S. (2002). A technical description of atmospheric sounding by GPS occultation. *Journal of Atmospheric and Solar-Terrestrial Physics*, *64*(4), 451–469. https://doi.org/10.1016/s1364-6826(01)00114-6

Haldoupis, C. (2011). A tutorial review on sporadic E layers. *Aeronomy of the Earth's Atmosphere and Ionosphere*, 381–394. https://doi.org/10.1007/978-94-007-0326-1_29

Haldoupis, C., Meek, C., Christakis, N., Pancheva, D., & Bourdillon, A. (2006). Ionogram height–time–intensity observations of descending sporadic E layers at mid-latitude. *Journal of Atmospheric and Solar-Terrestrial Physics*, *68*(3–5), 539–557. https://doi.org/10.1016/j.jastp.2005.03.020

Haldoupis, C., Pancheva, D., Singer, W., Meek, C., & MacDougall, J. (2007). An explanation for the seasonal dependence of midlatitude sporadic E layers. *Journal of Geophysical Research*, *112*(A6). https://doi.org/10.1029/2007ja012322

Hall, S., McDonald, D., McGratten, G., & MacKenzie, E. (1971). Rocket observations of middle latitude sporadic E, magnetic fields, winds and ionization. *Planetary and Space Science*, *19*(10), 1319–1325. https://doi.org/10.1016/0032-0633(71)90186-3

Harding, B. J., Chau, J. L., He, M., Englert, C. R., Harlander, J. M., Marr, K. D., et al. (2021). Validation of ICON-MIGHTI thermospheric wind observations: 2. Green-line comparisons to specular meteor radars. *Journal of Geophysical Research: Space Physics*, *126*(3), e2020JA028947. https://doi.org/10.1029/2020ja028947

Harding, B. J., Makela, J. J., Englert, C. R., Marr, K. D., Harlander, J. M., England, S. L., & Immel, T. J. (2017). The MIGHTI wind retrieval algorithm: Description and verification. *Space Science Reviews*, *212*(1), 585–600. https://doi.org/10.1007/s11214-017-0359-3

Hocke, K., Igarashi, K., Nakamura, M., Wilkinson, P., Wu, J., Pavelyev, A., & Wickert, J. (2001). Global sounding of sporadic E layers by the GPS/MET radio occultation experiment. *Journal of Atmospheric and Solar-Terrestrial Physics*, *63*(18), 1973–1980. https://doi.org/10.1016/s1364-6826(01)00063-3

Huba, J., Krall, J., & Drob, D. (2019). Global ionospheric metal ion transport with SAMI3. *Geophysical Research Letters*, *46*(14), 7937–7944. https://doi.org/10.1029/2019gl083583

Immel, T. J., England, S., Mende, S., Heelis, R., Englert, C., & Edelstein, J. (2018). The Ionospheric Connection Explorer mission: Mission goals and design. *Space Science Reviews*, *214*(1), 1–36. https://doi.org/10.1007/s11214-017-0449-2

Jacobi, C., & Arras, C. (2019). Tidal wind shear observed by meteor radar and comparison with sporadic E occurrence rates based on GPS radio occultation observations. *Advances in Radio Science*, *17*, 213–224. https://doi.org/10.5194/ars-17-213-2019

Jin, H., Miyoshi, Y., Fujiwara, H., & Shinagawa, H. (2008). Electrodynamics of the formation of ionospheric wave number 4 longitudinal structure. *Journal of Geophysical Research*, *113*(A9). https://doi.org/10.1029/2008ja013301

Jin, H., Miyoshi, Y., Fujiwara, H., Shinagawa, H., Terada, K., Terada, N., & Saito, A. (2011). Vertical connection from the tropospheric activities to the ionospheric longitudinal structure simulated by a new Earth's whole atmosphere-ionosphere coupled model. *Journal of Geophysical Research*, *116*(A1). https://doi.org/10.1029/2010ja015925

Jin, H., Miyoshi, Y., Pancheva, D., Mukhtarov, P., Fujiwara, H., & Shinagawa, H. (2012). Response of migrating tides to the stratospheric sudden warming in 2009 and their effects on the ionosphere studied by a whole atmosphere-ionosphere model Gaia with cosmic and timed/Saber observations. *Journal of Geophysical Research*, *117*(A10). https://doi.org/10.1029/2012ja017650

Kobayashi, S., Ota, Y., Harada, Y., Ebita, A., Moriya, M., Onoda, H., et al. (2015). The JRA-55 reanalysis: General specifications and basic characteristics. *Journal of the Meteorological Society of Japan. Ser. II*, *93*(1), 5–48. https://doi.org/10.2151/jmsj.2015-001

Kopp, E. (1997). On the abundance of metal ions in the lower ionosphere. *Journal of Geophysical Research*, *102*(A5), 9667–9674. https://doi.org/10.1029/97ja00384

Larsen, M. (2002). Winds and shears in the mesosphere and lower thermosphere: Results from four decades of chemical release wind measurements. *Journal of Geophysical Research*, *107*(A8). SIA-28. https://doi.org/10.1029/2001ja000218

Larsen, M., Fukao, S., Yamamoto, M., Tsunoda, R., Igarashi, K., & Ono, T. (1998). The SEEK chemical release experiment: Observed neutral wind profile in a region of sporadic E. *Geophysical Research Letters*, *25*(11), 1789–1792. https://doi.org/10.1029/98gl00986

Liu, Y., Zhou, C., Tang, Q., Li, Z., Song, Y., Qing, H., et al. (2018). The seasonal distribution of sporadic E layers observed from radio occultation measurements and its relation with wind shear measured by TIMED/TIDI. *Advances in Space Research*, *62*(2), 426–439. https://doi.org/10.1016/j.asr.2018.04.026

MacLeod, M. A., Keneshea, T. J., & Narcisi, R. S. (1975). Numerical modelling of a metallic ion sporadic-E layer. *Radio Science*, *10*(3), 371–388. https://doi.org/10.1029/rs010i003p00371

Mathews, J. (1998). Sporadic E: Current views and recent progress. *Journal of Atmospheric and Solar-Terrestrial Physics*, *60*(4), 413–435. https://doi.org/10.1016/s1364-6826(97)00043-6

Miller, K., & Smith, L. (1978). Incoherent scatter radar observations of irregular structure in mid-latitude sporadic E layers. *Journal of Geophysical Research*, *83*(A8), 3761–3775. https://doi.org/10.1029/ja083ia08p03761

Miyoshi, Y., & Fujiwara, H. (2003). Day-to-day variations of migrating diurnal tide simulated by a GCM from the ground surface to the exobase. *Geophysical Research Letters*, *30*(15). https://doi.org/10.1029/2003gl017695

Miyoshi, Y., Pancheva, D., Mukhtarov, P., Jin, H., Fujiwara, H., & Shinagawa, H. (2017). Excitation mechanism of non-migrating tides. *Journal of Atmospheric and Solar-Terrestrial Physics*, *156*, 24–36. https://doi.org/10.1016/j.jastp.2017.02.012

Pfaff, R., Larsen, M., Abe, T., Habu, H., Clemmons, J., Freudenreich, H., et al. (2020). Daytime dynamo electrodynamics with spiral currents driven by strong winds revealed by vapor trails and sounding rocket probes. *Geophysical Research Letters*, *47*(15), e2020GL088803. https://doi.org/10.1029/2020gl088803

Raizada, S., Smith, J., Lautenbach, J., Aponte, N., Perillat, P., Sulzer, M., & Mathews, J. (2020). New lidar observations of ca+ in the mesosphere and lower thermosphere over Arecibo. *Geophysical Research Letters*, *47*(5), e2020GL087113. https://doi.org/10.1029/2020gl087113

Resende, L. C. A., Arras, C., Batista, I. S., Denardini, C. M., Bertollotto, T. O., & Moro, J. (2018). Study of sporadic e layers based on GPS radio occultation measurements and Digisonde data over the Brazilian region. *Annales Geophysicae*, *36*, 587–593. https://doi.org/10.5194/angeo-36-587-2018

Resende, L. C. A., Batista, I. S., Denardini, C. M., Carrasco, A. J., de Fátima Andrioli, V., Moro, J., & Chen, S. S. (2016). Competition between winds and electric fields in the formation of blanketing sporadic E layers at equatorial regions. *Earth Planets and Space*, *68*(1), 1–14. https://doi.org/10.1186/s40623-016-0577-z

Schreiner, W. S., Weiss, J., Anthes, R. A., Braun, J., Chu, V., & Fong, J. (2020). othersCOSMIC-2 radio occultation constellation: First results. *Geophysical Research Letters*, *47*(4), e2019GL086841. https://doi.org/10.1029/2019gl086841

Shinagawa, H. (2011). Ionosphere simulation. *Journal of NICT*, *56*(1–4), 199–207.

Shinagawa, H., Miyoshi, Y., Jin, H., & Fujiwara, H. (2017). Global distribution of neutral wind shear associated with sporadic E layers derived from GAIA. *Journal of Geophysical Research: Space Physics*, *122*(4), 4450–4465. https://doi.org/10.1002/2016ja023778

Smith, L. G. (1966). Rocket observations of sporadic E and related features of the E region. *Radio Science*, *1*(2), 178–186. https://doi.org/10.1002/rds196612178

Taguchi, S. (1961). World maps of FOES. *Journal of the Radio Research Laboratory*, *8*, 38.

Whitehead, J. (1961). The formation of the sporadic-E layer in the temperate zones. *Journal of Atmospheric and Terrestrial Physics*, *20*(1), 49–58. https://doi.org/10.1016/0021-9169(61)90097-6

Whitehead, J. (1989). Recent work on mid-latitude and equatorial sporadic-E. *Journal of Atmospheric and Terrestrial Physics*, *51*(5), 401–424. https://doi.org/10.1016/0021-9169(89)90122-0

Wickert, J., Michalak, G., Schmidt, T., Beyerle, G., Cheng, C.-Z., Healy, S. B., et al. (2009). Gps radio occultation: Results from CHAMP, GRACE and FORMOSAT-3/COSMIC. *Terrestrial, Atmospheric and Oceanic Sciences*, *20*(1), 35–50. https://doi.org/10.3319/tao.2007.12.26.01(f3c)

Wu, D. L., Ao, C. O., Hajj, G. A., de La Torre Juarez, M., & Mannucci, A. J. (2005). Sporadic E morphology from GPS-CHAMP radio occultation. *Journal of Geophysical Research*, *110*(A1). https://doi.org/10.1029/2004ja010701

Yu, B., Xue, X., Yue, X., Yang, C., Yu, C., Dou, X., et al. (2019). The global climatology of the intensity of the ionospheric sporadic e layer. *Atmospheric Chemistry and Physics*, *19*(6), 4139–4151. https://doi.org/10.5194/acp-19-4139-2019

Yue, X., Schreiner, W. S., Pedatella, N., Anthes, R. A., Mannucci, A. J., Straus, P. R., & Liu, J.-Y. (2014). Space weather observations by GNSS radio occultation: From FORMOSAT-3/COSMIC to FORMOSAT-7/COSMIC-2. *Space Weather*, *12*(11), 616–621. https://doi.org/10.1002/2014sw001133